Research Article | Vol. 29, No. 11 / 24 May 2021 / Optics Express 17387
Optics EXPRESS

Enhancement of the photocurrents injected in gapped graphene by the orthogonally polarized two-color laser field

YINFU ZHANG,[1,3] JIAPENG LI,[1,3] LIANG LI,[1] TENGFEI HUANG,[1] XIAOSONG ZHU,[1] PENGFEI LAN,[1,4] AND PEIXIANG LU[1,2,5]

[1]School of Physics and Wuhan National Laboratory for Optoelectronics, Huazhong University of Science and Technology, Wuhan 430074, China
[2]Hubei Key Laboratory of Optical Information and Pattern Recognition, Wuhan Institute of Technology, Wuhan 430205, China
[3]These authors contributed equally to this work
[4]pengfeilan@hust.edu.cn
[5]lupeixiang@hust.edu.cn

Abstract: We theoretically investigate the photocurrents injected in gapped graphene by the orthogonally polarized two-color laser field. Depending on the relative phase, the photocurrents can be coherently controlled by deforming the electron trajectory in the reciprocal space. Under the same field strength, the peak photocurrent in the orthogonally polarized two-color field is about 20 times larger than that for linearly polarized light, and about 3.6 times for elliptically polarized light. The enhancement of the photocurrent can be attributed to an obvious asymmetric distribution of the real population in the reciprocal space, which is sensitive to the waveform of the laser field and related to the quantum interference between the electron trajectories. Our work provides a noncontact method to effectively enhance the injected current in graphene.

1. Introduction

Electron transport in solids [1–5] is central to many optoelectronic devices. In the considerable studies of electronic transport, it is crucial to choose suitable contacts between biased materials and an external circuit [6–11]. However, the development of contacts often hinders the research in this area. Recently, a noncontact, all-optical method [12–20] has been developed to coherently control the residual photocurrents after laser excitation in solids. Limited by the resonant absorption of semiconductors and screening of metals, this method is applied difficultly in the intense laser field [20–23].

To overcome these difficulties, graphene is an excellent material to investigate the photocurrent. Graphene, as a monolayer two-dimensional (2D) material, has a honeycomb crystal structure with two sublattices in the unit cell. Accordingly, the first Brillouin zone (BZ) contains two nonequivalent Dirac points K and K' (see in Fig. 1(a)) in the reciprocal space. Due to its unique electron transport properties, graphene has aroused the intense interest for electronic device applications [24–29]. It has also become a typical platform to study the interactions between intense laser fields and solids because of the broadband and ultrafast optical response, weak screening and high damage threshold. Note that pristine graphene is a zero-bandgap material. We can also open its bandgap to a narrow gap by different methods including doping [30] or positioning on an incommensurate substrate [31,32]. Gapped graphene is chemically identical to the pristine graphene but its inversion symmetry is broken.

More recently, intense laser fields have been applied to inject the photocurrent in graphene [23,33,34]. By steering the waveform of linearly or elliptically polarized few-cycle pulses, the current can be controlled effectively. However, the current injected by linear and elliptic few-cycle

#426593 https://doi.org/10.1364/OE.426593
Journal © 2021 Received 30 Mar 2021; revised 7 May 2021; accepted 9 May 2021; published 20 May 2021

Optics EXPRESS

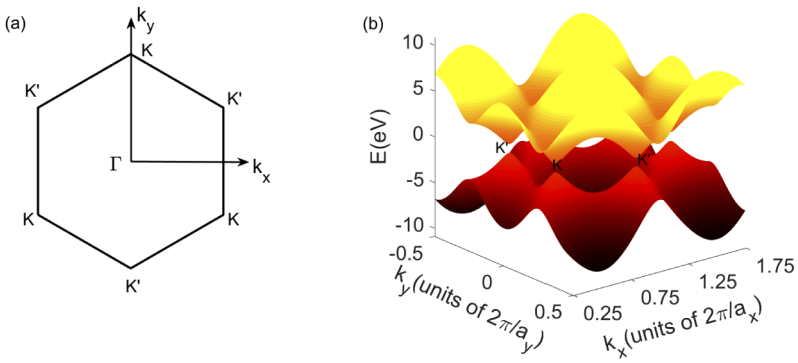

Fig. 1. (a) The first Brillouin zone of graphene with two valleys, K and K'. (b) The energy dispersion for gapped graphene with a band gap of 1 eV. a $_x$ and a $_y$ are the lattice constants in two directions.

laser pulses are relatively weak. Considering that the current is sensitive to the waveform of the laser field, an alternative solution to enhance the photocurrent is designing the waveform of the laser field. The fields with several different waveforms have been used in related studies. Single-cycle or few-cycle linearly polarized pulses are used to control the electron momentum distribution or valley polarization by steering the carrier envelope phase (CEP) [35,36]. The bicircular pulses are also used to control the asymmetric population [37,38]. In comparison of the linearly or elliptically polarized fields, orthogonally polarized two-color (OTC) fields show a greater asymmetry even with multi-cycle pulses and different circular polarization by steering the relative phase between the fundamental and second-harmonic fields. Due to these properties, the OTC field has been applied widely in interacting with gas medium [39–45], including high harmonic generation in gas and optical chirality.

In this paper, we propose a method to enhance the photocurrent in gapped graphene by the OTC field. The peak photocurrent in the OTC filed is obviously enhanced compared with linearly and elliptically polarized lights. We attribute the enhancement of the photocurrent to an obvious asymmetric real population in the reciprocal space. The asymmetric population is sensitive to the waveform of the laser field and related to the quantum interference of electron trajectories. In addition, the peak photocurrent can be controlled by changing the bandgap of gapped graphene. The OTC fields can induce a great asymmetry in the region near every K or K' point, respectively. This asymmetry is different from the valley polarization induced by bicircular pulses, which is the asymmetry between K and K' point.

2. Theoretical model

In the laser field, electron dynamics can be expressed by the time-dependent Schrödinger equation, which has the following form:

$$i\hbar\frac{d\psi}{dt} = H(t)\psi. \tag{1}$$

The total Hamiltonian $H(t)$ reads

$$H(t) = H_0 - e\mathbf{F}(t)\cdot\mathbf{r}, \tag{2}$$

where H_0 is the Hamiltonian of the solid in the absence of laser fields, e is the electron charge and $\mathbf{F}$ is the electric field. Atomic units are used throughout the paper unless otherwise stated. In our work, gapped graphene is considered as a 2D two-band model with the tight-binding approximation [46,47]. In this model, the hopping parameter is $\gamma = 3.03$ eV between nearest

Optics EXPRESS

neighboring atoms. The Hamiltonian is described by:

$$H_0 = \begin{pmatrix} \frac{\Delta}{2} & -\gamma f(\mathbf{k}) \\ -\gamma f^*(\mathbf{k}) & -\frac{\Delta}{2} \end{pmatrix}. \tag{3}$$

Here Δ is the finite gap between the valence band (VB) and the conduction band (CB), and

$$f(\mathbf{k}) = \exp(i\frac{ak_x}{\sqrt{3}}) + 2\exp(-i\frac{ak_x}{2\sqrt{3}})\cos(\frac{ak_y}{2})), \tag{4}$$

where $a = 0.246$ nm is the lattice constant of graphene. From the above Hamiltonian H_0, the energies of CB and VB can be obtained as follows:

$$E_c(\mathbf{k}) = +\sqrt{\gamma^2 |f(\mathbf{k})|^2 + \frac{\Delta^2}{4}}, \tag{5}$$

$$E_v(\mathbf{k}) = -\sqrt{\gamma^2 |f(\mathbf{k})|^2 + \frac{\Delta^2}{4}}, \tag{6}$$

where the footnotes of c and v stand for CB and VB, respectively. The energy dispersion of gapped graphene with $\Delta = 1$ eV is shown in Fig. 1(b).

In gapped graphene, the electron dynamics is driven by the laser field. According to the Bloch acceleration theorem [48], for an electron with an initial momentum $\mathbf{k}$, the time evolution of the crystal momentum $\mathbf{k}(t)$ can be expressed as:

$$\mathbf{k}(t) = \mathbf{k} - \mathbf{A}(t) \tag{7}$$

The corresponding adiabatic wave functions are the Houston functions [49],

$$\Phi_m^{(H)}(\mathbf{r}, t) = \Psi_{\mathbf{k}(t)}^{(m)}(\mathbf{r}) \exp\left[i\phi_m^{(D)}(\mathbf{k}(t)) + i\phi_m^{(B)}(\mathbf{k}(t))\right] \tag{8}$$

where $m = c, v$ for CB and VB, and $\Psi_{\mathbf{k}}^{(m)}$ are the Bloch-band eigenfunctions in the absence of the laser field. The dynamic phase $\phi_m^{(D)}$ and the geometric phase $\phi_m^{(B)}$ [50] are defined by the following expressions:

$$\phi_m^{(D)}(\mathbf{k}(t)) = -\frac{e}{\hbar}\int_{-\infty}^{t} E_m\left[\mathbf{k}(t')\right] dt' \tag{9}$$

$$\phi_m^{(B)}(\mathbf{k}(t)) = \frac{e}{\hbar}\int_{-\infty}^{t} \mathbf{F}(t')\mathbf{d}_{mm}\left[\mathbf{k}(t')\right] dt' \tag{10}$$

Here $\mathbf{d}_{mm}(\mathbf{k}) = \left\langle \Psi_{\mathbf{k}}^{(m)} \middle| i\frac{\partial}{\partial \mathbf{k}} \middle| \Psi_{\mathbf{k}}^{(m)} \right\rangle$ is the intraband connection for band m.

By solving the 2D two-band density matrix equations (DMEs) [51–54], the response of the laser-driven electron in a crystal can be described as follows:

$$\dot{\Pi}(\mathbf{k}(t)) = -\frac{\Pi(\mathbf{k}(t))}{T_2} - i\Omega(\mathbf{k}(t))\alpha(\mathbf{k}(t))e^{-i(S_1+S_2))}, \tag{11}$$

$$\dot{n}_c(\mathbf{k}(t)) = i\Omega^*(\mathbf{k}(t))\Pi(\mathbf{k}(t))e^{i(S_1+S_2)} + c.c., \tag{12}$$

$$\dot{n}_v(\mathbf{k}(t)) = -i\Omega^*(\mathbf{k}(t))\Pi(\mathbf{k}(t))e^{i(S_1+S_2)} + c.c., \tag{13}$$

where n_c and n_v are the populations of CB and VB, respectively. Π is the off-diagonal element of the density matrix. $\alpha = n_v - n_c$ is the population difference between VB and CB. T_2 is the

Optics EXPRESS

dephasing time stemming from the coherence decay in solids. Based on Ref. [55], the dephasing time is 35 fs in our calculation. The phase difference is $S_1 = \phi_c^{(D)} - \phi_v^{(D)}$ and $S_2 = \phi_c^{(B)} - \phi_v^{(B)}$. Ω is the Rabi frequency, given by $\Omega(\mathbf{k}(t)) = -i\mathbf{F}(t) \cdot \mathbf{d}_{cv}(\mathbf{k})$. $\mathbf{d}_{cv}$ is the dipole matrix element between the conduction and valence states [56–58]:

$$\mathbf{d}_{cv}(\mathbf{k}) = \left\langle \psi_{\mathbf{k}}^{(c)} \right| i\frac{\partial}{\partial \mathbf{k}} \left| \psi_{\mathbf{k}}^{(v)} \right\rangle. \tag{14}$$

After the pulsed interaction, the real population on CB is defined as $N_c(\mathbf{k})$. According to Ref. [33], the residual photocurrent after laser excitation in the first Brillouin zone (BZ) can be estimated as the following:

$$J = \frac{l}{D} \int_{BZ} 2^2 N_c(\mathbf{k}) \frac{\partial \mathbf{E}(\mathbf{k})}{\partial \mathbf{k}} \tau_1 d\mathbf{k}, \tag{15}$$

Here we choose the value of ballistic lifetime $\tau_1 = 40$ fs based on previous researches [59–61]. The diffusion constant D equals 1.1×10^4 cm^{2}s^{-1} and the diffusion length l is about 0.35 μm.

3. Results and discussion

We apply an OTC laser pulse incident normally to the gapped graphene. The electric field of this pulse is described as

$$\mathbf{F}_1(t) = -\mathbf{e}_{k_x} F_{0x} g(t) \cos(2\omega t + \phi) + \mathbf{e}_{k_y} F_{0y} g(t) \cos(\omega t), \tag{16}$$

where ω is the fundamental frequency. Considering the value of current and the damage threshold of graphene, we choose the fundamental laser with $\lambda = 4700$ nm. $\mathbf{e}_{k_x}$ and $\mathbf{e}_{k_y}$ are the unit vectors along $\mathbf{k}_x$ and $\mathbf{k}_y$. The field amplitudes $F_{0x} = F_{0y} = \sqrt{I}$, where I=0.34 TW/cm^2, and ϕ is the relative phase between the two components. The time-envelope of the pulses has the following expression:

$$g(t) = \exp(-2ln2 \cdot \frac{t^2}{\tau^2}), \tag{17}$$

where the full width at half maximum $\tau = 2.5T_0$. T_0 is the optical cycle of second harmonic pulses. For the elliptically and linearly polarized fields, they have the following expressions:

$$\mathbf{F}_2(t) = -\mathbf{e}_{k_x} F_{0x} g(t) \cos(2\omega t + \phi) + \mathbf{e}_{k_y} F_{0y} g(t) \cos(2\omega t), \tag{18}$$

$$\mathbf{F}_3(t) = -\sqrt{2}\mathbf{e}_{k_x} F_{0x} g(t) \cos(2\omega t + \phi). \tag{19}$$

The photocurrents along $\mathbf{k}_x$ induced by OTC, elliptically and linearly polarized fields are shown as blue, orange and purple dot-dash lines in Fig. 2(a), respectively. For the OTC field, the current is tunable with steering the relative phase. When $\phi = -0.5\pi$, the photocurrent reaches the maximum. The direction of the current is reversal at $\phi = 0$. For the elliptically polarized light, we also observe the oscillating current by changing the relative phase. However, the peak current is only about 0.38 nA. For the linearly polarized field, the current shows a weak modulation and the maximum is just 0.07 nA. Compared with the currents in the elliptically polarized field and the linearly polarized field, the peak current in the OTC field is about 3.6 and 20 times larger than that in the two else fields, respectively. We also show the photocurrents along $\mathbf{k}_y$ in Fig. 2(b). Similarly, the peak current in the OTC field is higher than that in the linearly and the elliptically polarized fields.

To understand the mechanism of the peak current enhancement, we show the real population in the linearly ($\phi = -0.5\pi$), elliptically polarized ($\phi = -0.75\pi$) and OTC field ($\phi = -0.5\pi$, 0) in Figs. 3(a)-(d), respectively. The inset figures are the vector potential of the laser field. The

Optics EXPRESS

excited electrons are mainly distributed around K and K'. In Fig. 3(a), one can see a bright area of the population along a straight line whose center is K or K'. In Fig. 3(b), the population exhibits bright circles around K and K'. In Fig. 3(c), the population follows a C shape. In the OTC field at $\phi = 0$, the population exhibits a figure-eight shape in Fig. 3(d). These results clearly show that the population has a similar shape to the waveform of the laser field. Compared with straight lines, circles and the figure-eight shape, the C shape of the population exhibits the most obvious asymmetry in $\mathbf{k}_x$ direction.

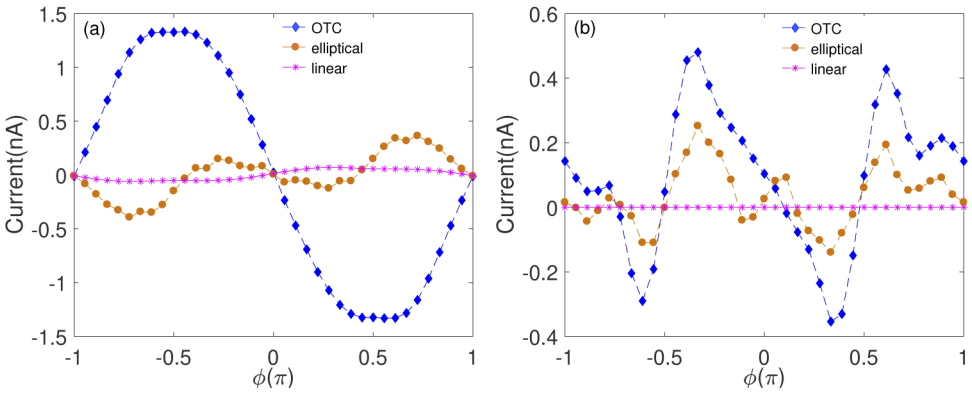

Fig. 2. The photocurrents as a function of the relative phase ϕ in several different fields along (a) $\mathbf{k}_x$ and (b) $\mathbf{k}_y$. In the linearly polarized field, ϕ indicates the carrier-envelope-phase (CEP).

Note that the population near every K and K' point is asymmetric. To quantify this asymmetry, we choose the real population distribution around K. Taking account of the dashed region (see in Fig. 3(c)), we define the asymmetry along $\mathbf{k}_x$ and $\mathbf{k}_y$ as

$$\begin{aligned} \eta_x &= \frac{n_1 - n_2}{n_1 + n_2} \times 100\%, \\ \eta_y &= \frac{n_3 - n_4}{n_3 + n_4} \times 100\%, \end{aligned} \tag{20}$$

respectively. n_1 (n_2) is the sum of the population where $-0.25<\mathbf{k}_x<0$ ($0<\mathbf{k}_x<0.25$) and n_3 (n_4) is the sum of the population where $0.33<\mathbf{k}_y<0.5$ ($0.17<\mathbf{k}_y<0.33$) (see in Fig. 4). As illustrated in Fig. 4(a), the maximum of η_x is close to 9% in the linearly or elliptically polarized fields. Whereas, the peak η_x can be enhanced to 24% in the OTC field. Moreover, η_y shown in Fig. 4(b) also exhibits a similar enhancement as a function of the relative phase. In comparison of the photocurrents and the population asymmetry (see Figs. 2 and 4), one can see that they have similar dependence on phase. In other words, the photocurrents and the population asymmetry have a strong relevance. The higher the population asymmetry, the larger the photocurrent output will be.

Next we have a deeper insight into the asymmetric population along $\mathbf{k}_x$ and $\mathbf{k}_y$ in the following respectively. Along $\mathbf{k}_x$, we choose two points P_1 and P_3 around K in the OTC field at $\phi = -0.5\pi$. As indicated in Fig. 5(a), P_1 is located on the bright fringes with large population. P_3 situates to the left of point K where the population is small. In Fig. 5(b), we define the parameter $I(t_i) = |\chi(t_i)|^2$, which is proportional to the ionization probability. The complex amplitude of ionization rate $\chi(t_i)$ is defined as [52,53]:

$$\chi(t_i) = -i\mathbf{d}_{cv}(\mathbf{k}(t_i)) \cdot \mathbf{F}(t_i) \cdot e^{i(S_1(t_i)+S_2(t_i))}. \tag{21}$$

Optics EXPRESS

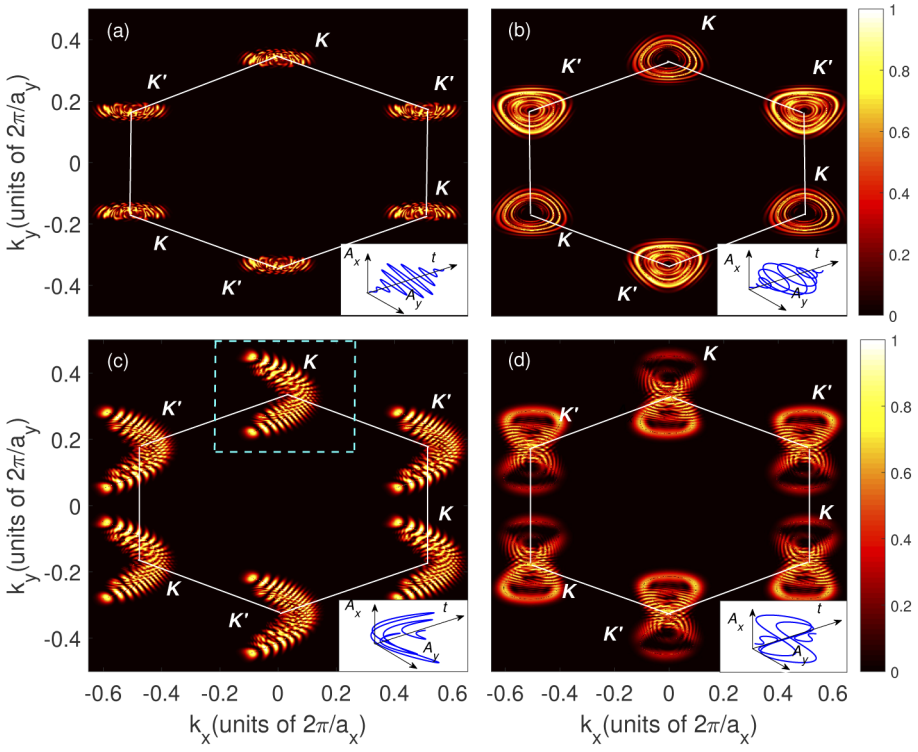

Fig. 3. Real population of gapped graphene in the reciprocal space (a) in the linearly polarized field at CEP = -0.5π, (b) in the elliptically polarized field at $\phi = -0.75\pi$, (c) in the OTC field at $\phi = -0.5\pi$ and (d) in the OTC field at $\phi = 0$. The corresponding vector fields are shown in the inset figures.

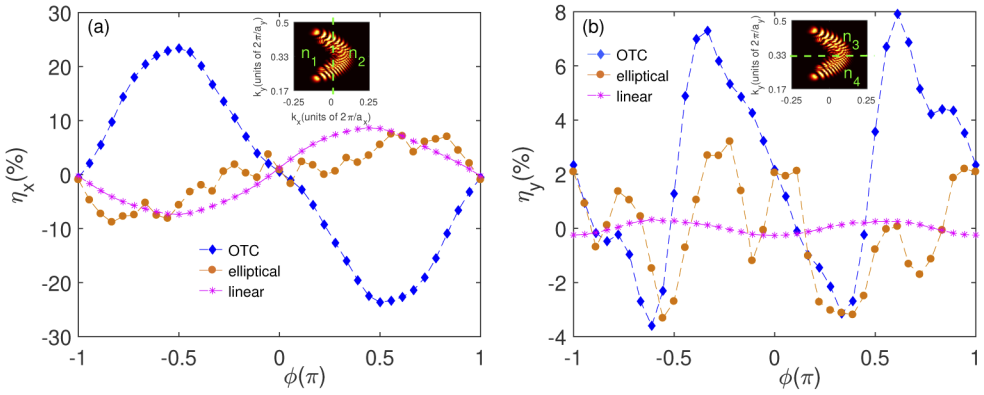

Fig. 4. The asymmetry of the real population as a function of CEP or the relative phase. η_x and η_y are defined as $\frac{n_1-n_2}{n_1+n_2} \times 100\%$ and $\frac{n_3-n_4}{n_3+n_4} \times 100\%$, respectively. n_1, n_2, n_3 and n_4 are indicated in inset figures.

Optics EXPRESS

One can see that I almost maintains zero for electrons with the initial momentum P_3, which leads to the little accumulation of the population. In contrast, I raises up obviously at time t_1 and t_3 for electrons with the initial momentum P_1 and reaches about 3 at the end of the OTC field.

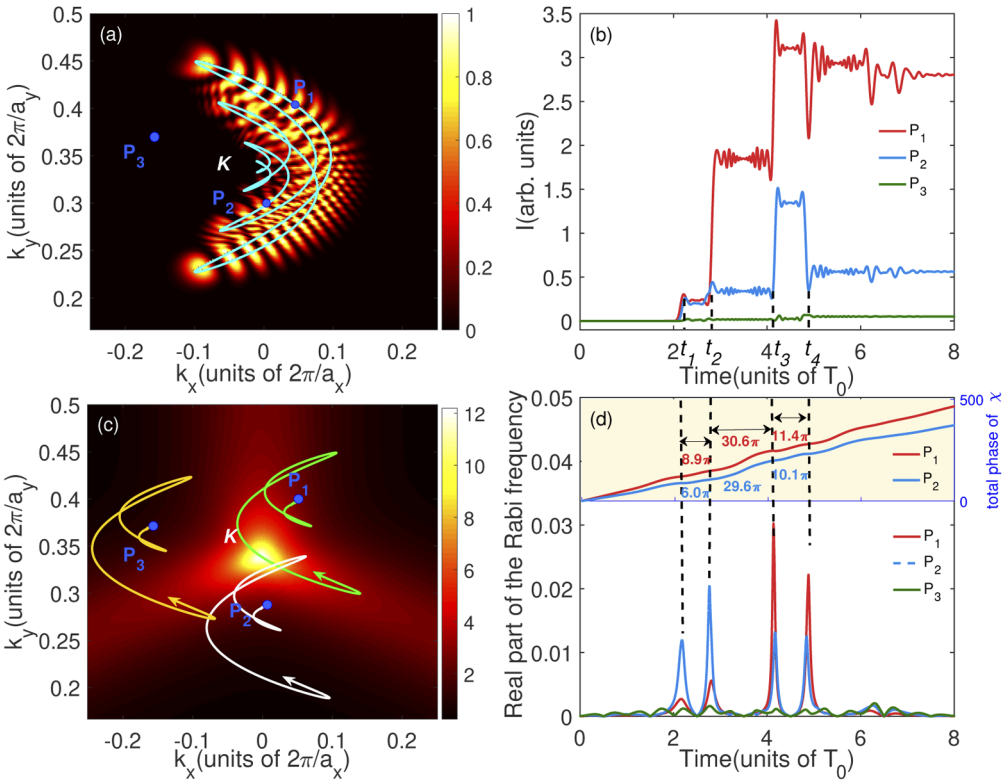

Fig. 5. The analysis of ionization, dynamic trajectories and inteference for three typical points in the reciprocal space. (a) Three points chosen to analyse in the reciprocal space. The three points are indicated as blue dots, P_1, P_2 and P_3. The field of the vector potential is shown as the blue curve. (b) The parameter I of P_1, P_2 and P_3 as a function of time. I is defined as $|\chi(t_i)|^2$, which is proportional to the ionization probability. (c) The trajectories of electrons with the three initial momentum P_1, P_2 and P_3 in the reciprocal space. The real part of $\mathbf{d}_{cv}(\mathbf{k})$ is shown as the background figure with a colorbar. (d) The real part of the Rabi frequency and the phase of ionization rate for the three points.

When solids are irradiated by a laser pulse, electrons oscillate on VB before excited into CB. In this pre-acceleration process [52], an electron with a large real part of $\mathbf{d}_{cv}$ has a higher probability to be excited. We show the real part of $\mathbf{d}_{cv}$ in Fig. 5(c). Note that it reaches the maximum near K. Meanwhile, the electron trajectories ($\mathbf{k} = \mathbf{k}_0 - \mathbf{A}(t)$) of P_1 and P_3 are plotted as green and yellow curves. One can see that the trajectory of P_1 passes through K, but that of P_3 keeps away from K. In consequence, the elelctron at P_3 is hardly to be excited due to the small real part of $\mathbf{d}_{cv}$. Whereas, the electrons passing through K have a large probability to be excited into CB. These electrons populated on CB form a similar shape of the vector potential (see the blue curve in Fig. 5(a)).

Then we focus on the asymmetric population along $\mathbf{k}_y$. Different from that in $\mathbf{k}_x$ direction, the OTC field has a good symmetry along $\mathbf{k}_y$. The enhancement of photocurrents in $\mathbf{k}_y$ direction is due to another mechanism. As illustrated in Figs. 3(c) and (d), one can see many bright fringes of the population. We choose P_1 and P_2 to discuss the enhanced photocurrents along $\mathbf{k}_y$. As

Optics EXPRESS

indicated in Fig. 5(a), P_2 is located in the interval between the fringes with small population. We show the parameter I of electrons with the initial momentum P_2 in Fig. 5(b). Comparing electrons of P_1 and P_2, they have obvious differences in the excitation process. At time t_2, I of P_1 raises up from 0.2 to 1.9, while that of P_2 keeps about 0.4. After time t_4, I of P_1 oscillates around 3, whereas I of P_2 decreases rapidly. Futhermore, the real part of the Rabi frequency between CB and VB is shown in Fig. 5(d). For P_1 and P_2, the real part of the Rabi frequency peaks at t_1, t_2, t_3 and t_4. Electrons excited at these time dominate the ionization process and interfere with each other. The interference between electron excition at time t_1 and t_2 belongs to the intracycle interference [62]. Similar to Eq. (21), the complex amplitude of electron excition at time t_1 and t_2 can be described by $\chi(t_1)$ and $\chi(t_2)$. The intensity of interference is proportional to $(1 - e^{i\Delta S})$, where ΔS is the difference of total phase between t_1 and t_2. Note that total phase includes S_1, S_2 and the phase of $\mathbf{d}_{cv}$. When ΔS is an integral multiple of 2π, electron excition is suppressed [62]. As shown in the upper part of Fig. 5(d), the curves depict the total phase of $\chi(t_i)$. Note that ΔS is 8.9π for P_1 and 6.0π for P_2. This makes a drop of I for P_2 at t_2 shown in Fig. 5(b). Similarly, an obvious decrease exists at time t_4 for P_2 because ΔS is 10.1π between t_3 and t_4. Due to the different gathered phase for electrons, the asymmetric interference fringes of the population arises. They result in the enhancement of the photocurrent along $\mathbf{k}_y$.

We also investigate the population in the OTC field at $\phi = 0$ in Fig. 6. Similarly, we select P_4 and P_5 on the each side of K along $\mathbf{k}_x$ in Fig. 6(a). As shown in Fig. 6(b), I of P_4 is almost as large as that of P_5. This leads to the symmetric population. As a result, the current injected by the OTC field at $\phi = 0$ is much lower than that at $\phi = -0.5\pi$. By steering the relative phase, we can control the current effectively.

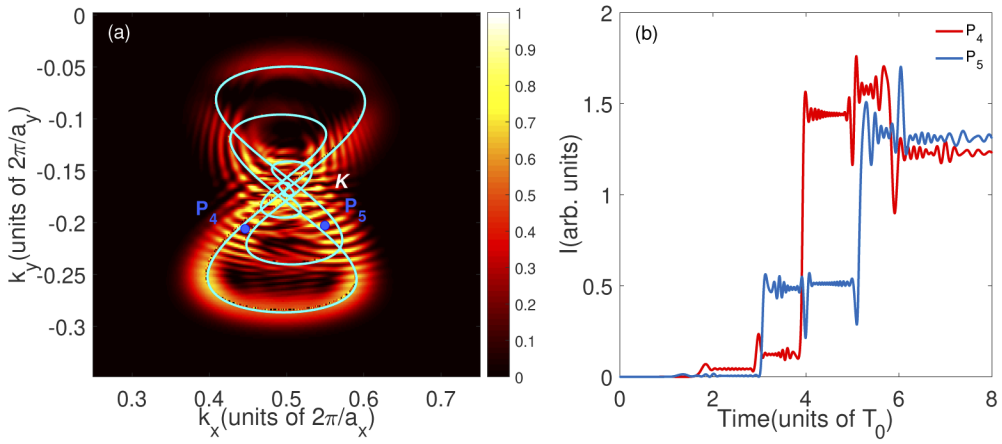

Fig. 6. (a) The real population in the OTC field at $\phi = 0$. (b) I of electrons with initial momentum P_4 and P_5.

In addition, the photocurrent is related to the bandgap of gapped graphene. In gapped graphene with different bandgaps, the photocurrent induced by the OTC field at $\phi = -0.5\pi$ is shown in Fig. 7. The current keeps larger than 1.2 nA when 0 eV $<\Delta<$ 1 eV and achieves its maximum near $\Delta = 1$ eV. Once Δ is more than 1 eV, the current drops rapidly. This may be related to the low ionization probability. It implies that one can control the photocurrent injected in gapped graphene by steering the bandgap except for the relative phase of the OTC field. Besides, we also simulate the current as a function of the bandgap for different intensities and frequencies. The general tendency of the current is similar as the conclusion of Fig. 7. For a higher intensity, the current is increased and achieves its maximum at a smaller gap. The current decreases by using OTC fields with shorter wavelengths.

Optics EXPRESS

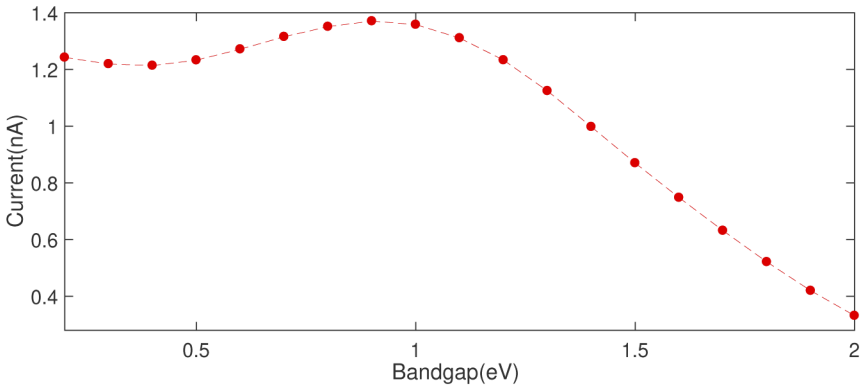

Fig. 7. The photocurrent induced by the OTC field at $\phi = -0.5\pi$ in gapped graphene with different gaps.

4. Conclusion

In summary, we investigate the photocurrent injected in gapped graphene by the OTC field. Compared with the linearly and ellipitically polarized fields, the photocurrent injected by the OTC field increases by 20 times and 3.6 times respectively. We attribute the enhancement to a stronger asymmetry of the population on CB and the quantum interference between electron trajectories. In addition, the photocurrent is also impacted by the bandgap of gapped graphene except for the relative phase of the field. These results indicate that one can inject the photocurrent in gapped graphene by the OTC field effectively and control the strength and direction of the current by steering the relative phase or the bandgap.

Funding. Science and Technology Planning Project of Guangdong Province (2018B090944001); National Natural Science Foundation of China (91950202, 11627809, 11874165, 11774109, 11934006, 12021004).

Disclosures. The authors declare no conflicts of interest.

Data availability. Data underlying the results presented in this paper are not publicly available at this time but may be obtained from the authors upon reasonable request.

References

1. C. Berger, Z. Song, X. Li, X. Wu, N. Brown, C. Naud, D. Mayou, T. Li, J. Hass, A. N. Marchenkov, E. H. Conrad, P. N. First, and W. A. de Heer, "Electronic confinement and coherence in patterned epitaxial graphene," Science **312**(5777), 1191–1196 (2006).
2. K. I. Bolotin, K. J. Sikes, J. Hone, H. L. Stormer, and P. Kim, "Temperature-dependent transport in suspended graphene," Phys. Rev. Lett. **101**(9), 096802 (2008).
3. S. V. Morozov, K. S. Novoselov, M. I. Katsnelson, F. Schedin, D. C. Elias, J. A. Jaszczak, and A. K. Geim, "Giant intrinsic carrier mobilities in graphene and its bilayer," Phys. Rev. Lett. **100**(1), 016602 (2008).
4. M. Orlita, C. Faugeras, P. Plochocka, P. Neugebauer, G. Martinez, D. K. Maude, A.-L. Barra, M. Sprinkle, C. Berger, W. A. de Heer, and M. Potemski, "Approaching the dirac point in high-mobility multilayer epitaxial graphene," Phys. Rev. Lett. **101**(26), 267601 (2008).
5. X. Han, K. Wang, P. D. Persaud, X. Xing, W. Liu, H. Long, F. Li, B. Wang, M. R. Singh, and P. Lu, "Harmonic resonance enhanced second-harmonic generation in the monolayer WS_2-Ag nanocavity," ACS Photonics **7**(3), 562–568 (2020).
6. A. Cottet, T. Kontos, S. Sahoo, H. T. Man, M.-S. Choi, W. Belzig, C. Bruder, A. F. Morpurgo, and C. Schönenberger, "Nanospintronics with carbon nanotubes," Semicond. Sci. Technol. **21**(11), S78–S95 (2006).
7. M. S. Purewal, B. H. Hong, A. Ravi, B. Chandra, J. Hone, and P. Kim, "Scaling of resistance and electron mean free path of single-walled carbon nanotubes," Phys. Rev. Lett. **98**(18), 186808 (2007).
8. H. B. Heersche, P. J. Herrero, J. B. Oostinga, L. M. K. Vandersypen, and A. F. Morpurgo, "Bipolar supercurrent in graphene," Nature **446**(7131), 56–59 (2007).
9. N. Katzenellenbogen and D. Grischkowsky, "Efficient generation of 380 fs pulses of THz radiation by ultrafast laser-pulse excitation of a biased metal-semiconductor interface," Appl. Phys. Lett. **58**(3), 222–224 (1991).
10. T. Nagatsuma, "Photonic measurement technologies for high-speed electronics," Meas. Sci. Technol. **13**(11), 1655–1663 (2002).

Optics EXPRESS

11. G. C. Valley, "Photonic analog-to-digital converters," Opt. Express **15**(5), 1955–1982 (2007).
12. G. Kurizki, M. Shapiro, and P. Brumer, "Phase-coherent control of photocurrent directionality in semiconductors," Phys. Rev. B **39**(5), 3435–3437 (1989).
13. R. Atanasov, A. Hache, J. L. P. Hughes, H. M. van Driel, and J. E. Sipe, "Coherent control of photocurrent generation in bulk semiconductors," Phys. Rev. Lett. **76**(10), 1703–1706 (1996).
14. I. Franco, M. Shapiro, and P. Brumer, "Robust ultrafast currents in molecular wires through stark shifts," Phys. Rev. Lett. **99**(12), 126802 (2007).
15. Y. V. Pershin and C. Piermarocchi, "Radiation-induced current in quantum wires with side-coupled nanorings," Phys. Rev. B **75**(3), 035326 (2007).
16. D. Sun, C. Divin, J. Rioux, J. E. Sipe, C. Berger, W. A. de Heer, P. N. First, and T. B. Norris, "Coherent control of ballistic photocurrents in multilayer epitaxial graphene using quantum interference," Nano Lett. **10**(4), 1293–1296 (2010).
17. R. W. Newson, J. M. Ménard, C. Sames, M. Betz, and H. M. van Driel, "Coherently controlled ballistic charge currents injected in single-walled carbon nanotubes and graphite," Nano Lett. **8**(6), 1586–1589 (2008).
18. L. Costa, M. Betz, M. Spasenovic, A. D. Bristow, and H. M. van Driel, "All-optical injection of ballistic electrical currents in unbiased silicon," Nat. Phys. **3**(9), 632–635 (2007).
19. L. Prechtel, L. Song, S. Manus, D. Schuh, W. Wegscheider, and A. W. Holleitner, "Time-resolved picosecond photocurrents in contacted carbon nanotubes," Nano Lett. **11**(1), 269–272 (2011).
20. A. Schiffrin, T. Paasch-Colberg, N. Karpowicz, V. Apalkov, D. Gerster, S. Mühlbrandt, M. Korbman, J. Reichert, M. Schultze, S. Holzner, J. V. Barth, R. Kienberger, R. Ernstorfer, V. S. Yakovlev, M. I. Stockman, and F. Krausz, "Optical-field-induced current in dielectrics," Nature **493**(7430), 70–74 (2013).
21. J. D. Jackson, *Classical Electrodynamics*, 3rd ed. (Wiley, New York, NY, 1999).
22. F. Krausz and M. I. Stockman, "Attosecond metrology: from electron capture to future signal processing," Nat. Photonics **8**(3), 205–213 (2014).
23. C. Heide, T. Higuchi, H. B. Weber, and P. Hommelhoff, "Coherent electron trajectory control in graphene," Phys. Rev. Lett. **121**(20), 207401 (2018).
24. C. Berger, Z. Song, T. Li, X. Li, A. Y. Ogbazghi, R. Feng, Z. Dai, A. N. Marchenkov, E. I. I.. Conrad, P. N. First, and W. A. de Ileer, "Ultrathin epitaxial graphite: 2D electron gas properties and a route toward graphene-based nanoelectronics," J. Phys. Chem. B **108**(52), 19912–19916 (2004).
25. W. A. de Heer, C. Berger, X. Wu, P. N. First, E. H. Conrada, X. Li, T. Li, M. Sprinkle, J. Hass, M. L. Sadowski, M. Potemski, and G. Martinez, "Epitaxial graphene," Solid State Commun. **143**(1-2), 92–100 (2007).
26. A. K. Geim and K. S. Novoselov, "The rise of graphene," Nat. Mater. **6**(3), 183–191 (2007).
27. K. S. Novoselov, A. K. Geim, S. V. Morozov, D. Jiang, Y. Zhang, S. V. Dubonos, I. V. Grigorieva, and A. A. Firsov, "Electric field effect in atomically thin carbon films," Science **306**(5696), 666–669 (2004).
28. F. Wang, Y. Zhang, C. Tian, C. Girit, A. Zettl, M. Crommie, and Y. R. Shen, "Gate-variable optical transitions in graphene," Science **320**(5873), 206–209 (2008).
29. Y. Zhang, T. Tang, C. Girit, Z. Hao, M. C. Martin, A. Zettl, M. F. Crommie, Y. R. Shen, and F. Wang, "Direct observation of a widely tunable bandgap in bilayer graphene," Nature **459**(7248), 820–823 (2009).
30. T. Ohta, A. Bostwick, T. Seyller, K. Horn, and E. Rotenberg, "Controlling the electronic structure of bilayer graphene," Science **313**(5789), 951–954 (2006).
31. M. S. Nevius, M. Conrad, F. Wang, A. Celis, M. N. Nair, A. T. Ibrahimi, A. Tejeda, and E. H. Conrad, "Semiconducting graphene from highly ordered substrate interactions," Phys. Rev. Lett. **115**(13), 136802 (2015).
32. D. Jariwala, A. Srivastava, and P. M. Ajayan, "Graphene synthesis and band gap opening," J. Nanosci. Nanotechnol. **11**(8), 6621–6641 (2011).
33. T. Higuchi, C. Heide, K. Ullmann, H. B. Weber, and P. Hommelhoff, "Light-field-driven currents in graphene," Nature **550**(7675), 224–228 (2017).
34. S. A. O. Motlagh, F. Nematollahi, A. Mitra, A. J. Zafar, V. Apalkov, and M. I Stockman, "Ultrafst optical currents in gapped graphene," J. Phys.: Condens. Matter **32**(6), 065305 (2020).
35. C. Lefebvre, D. Gagnon, F. Fillion-Gourdeau, and S. Maclean, "Carrier-envelope phase effects in graphene," J. Opt. Soc. Am. B **35**(4), 958–966 (2018).
36. Á. Jiménez-Galán, R. E. F. Silva, O. Smirnova, and M. Ivanov, "Sub-cycle valleytronics: control of valley polarization using few-cycle linearly polarized pulses," Optica **8**(3), 277–280 (2021).
37. T. Nag, R.-J. Slager, T. Higuchi, and T. Oka, "Dynamical synchronization transition in interacting electron systems," Phys. Rev. B **100**(13), 134301 (2019).
38. Á. Jiménez-Galán, R. E. F. Silva, O. Smirnova, and M. Ivanov, "Lightwave control of topological properties in 2D materials for sub-cycle and non-resonant valley manipulation," Nat. Photonics **14**(12), 728–732 (2020).
39. C. Zhai, X. Zhang, X. Zhu, L. He, Y. Zhang, B. Wang, Q. Zhang, P. Lan, and P. Lu, "Single-shot molecular orbital tomography with orthogonal two-color fields," Opt. Express **26**(3), 2775–2784 (2018).
40. D. Shafir, H. Soifer, B. D. Bruner, M. Dagan, Y. Mairesse, S. Patchkovskii, M. Y. Ivanov, O. Smirnova, and N. Dudovich, "Resolving the time when an electron exits a tunnelling barrier," Nature **485**(7398), 343–346 (2012).
41. G. Vampa, T. J. Hammond, N. Thiré, B. E. Schmidt, F. Légaré, C. R. McDonald, T. Brabec, and P. B. Corkum, "Linking high harmonics from gases and solids," Nature **522**(7557), 462–464 (2015).

Optics EXPRESS

42. J. Chen, M. Han, X. Xiao, L. Peng, and Y. Liu, "Resolving the time when an electron exits a tunnelling barrier," Phys. Rev. A **98**(3), 033403 (2018).
43. P. V. Demekhin, A. N. Artemyev, A. Kastner, and T. Baumert, "Photoelectron circular dichroism with two overlapping laser pulses of carrier frequencies ω and 2ω linearly polarized in two mutually orthogonal directions," Phys. Rev. Lett. **121**(25), 253201 (2018).
44. S. Rozen, A. Comby, E. Bloch, S. Beauvarlet, D. Descamps, B. Fabre, S. Petit, V. Blanchet, B. Pons, N. Dudovich, and Y. Mairesse, "Controlling subcycle optical chirality in the photoionization of chiral molecules," Phys. Rev. X **9**(3), 031004 (2019).
45. C. Zhai, R. Shao, P. Lan, B. Wang, Y. Zhang, H. Yuan, N. M. Stephen, L. He, and P. Lu, "Ellipticity control of high-order harmonic generation with nearly orthogonal two-color laser fields," Phys. Rev. A **101**(5), 053407 (2020).
46. T. G. Pedersen, A.-P. Jauho, and K. Pedersen, "Optical response and excitons in gapped graphene," Phys. Rev. B **79**(11), 113406 (2009).
47. S. A. O. Motlagh, F. Nematollahi, V. Apalkov, and M. I Stockman, "Topological resonance and single-optical-cycle valley polarization in gapped graphene," Phys. Rev. B **100**(11), 115431 (2019).
48. F. Bloch, "Über die Quantenmechanik der Elektronen in Kristallgittern," Eur. Phys. J. A **52**(7-8), 555–600 (1929).
49. W. V. Houston, "Acceleration of electrons in a crystal lattice," Phys. Rev. **57**(3), 184–186 (1940).
50. M. V. Berry, "Quantal phase factors accompanying adiabatic changes," Proc. R. Soc. London, Ser. A **392**(1802), 45–57 (1984).
51. G. Vampa, C. R. McDonald, G. Orlando, D. D. Klug, P. B. Corkum, and T. Brabec, "Theoretical analysis of high-harmonic generation in solids," Phys. Rev. Lett. **113**(7), 073901 (2014).
52. L. Li, P. Lan, X. Zhu, T. Huang, Q. Zhang, M. Lein, and P. Lu, "Reciprocal-Space-Trajectory perspective on high-harmonic generation in solids," Phys. Rev. Lett. **122**(19), 193901 (2019).
53. G. Vampa, C. R. McDonald, G. Orlando, P. B. Corkum, and T. Brabec, "Semiclassical analysis of high harmonic generation in bulk crystals," Phys. Rev. B **91**(6), 064302 (2015).
54. X. Liu, L. Li, X. Zhu, T. Huang, X. Zhang, D. Wang, P. Lan, and P. Lu, "Wavelength dependence of high-order harmonic yields in solids," Phys. Rev. A **98**(6), 063419 (2018).
55. C. Liu, Y. Zheng, Z. Zeng, and R. Li, "Driving-laser ellipticity dependence of high-order harmonic generation in graphene," Phys. Rev. A **97**(6), 063412 (2018).
56. F. Wilczek and A. Zee, "Appearance of gauge structure in simple dynamical systems," Phys. Rev. Lett. **52**(24), 2111–2114 (1984).
57. D. Xiao, M. C. Chang, and Q. Niu, "Berry phase effects on electronic properties," Rev. Mod. Phys. **82**(3), 1959–2007 (2010).
58. F. Yang and R. B. Liu, "Nonlinear optical response induced by non-Abelian Berry curvature in time-reversal-invariant insulators," Phys. Rev. B **90**(24), 245205 (2014).
59. M. Breusing, S. Kuehn, T. Winzer, E. Malić, F. Milde, N. Severin, J. P. Rabe, C. Ropers, A. Knorr, and T. Elsaesser, "Ultrafast nonequilibrium carrier dynamics in a single graphene layer," Phys. Rev. B **83**(15), 153410 (2011).
60. I. Gierz, J. C. Petersen, M. Mitrano, C. Cacho, I. C. Edmond Turcu, E. Springate, A. Stöhr, A. Köhler, U. Starke, and A. Cavalleri, "Snapshots of non-equilibrium Dirac carrier distributions in graphene," Nat. Mater. **12**(12), 1119–1124 (2013).
61. K. J. Tielrooij, L. Piatkowski, M. Massicotte, A. Woessner, Q. Ma, Y. Lee, K. S. Myhro, C. N. Lau, P. Jarillo-Herrero, N. F. van Hulst, and F. H. L. Koppens, "Generation of photovoltage in graphene on a femtosecond timescale through efficient carrier heating," Nat. Nanotechnol. **10**(5), 437–443 (2015).
62. J. Li, L. Li, Q. Zhang, X. Zhu, T. Huang, P. Lan, and P. Lu, "Channel-closing effects of electronic excitation in solids," Opt. Express **27**(26), 37224–37235 (2019).